Step-Edge Induced Anisotropic Domain-Wall Propagation

P. Haibach, M. Huth, and H. Adrian
Institut für Physik, Johannes Gutenberg-Universität Mainz, D-55099 Mainz, Germany
(Received 9 July 1999)

We report the observation of anisotropic domain-wall propagation in ultrathin magnetic films with perpendicular anisotropy. A controlled density of step edges was introduced which allowed us to quantify its influence on the domain-wall pinning. For a sawtooth arrangement of the step edges the corresponding wall movement resulted in triangular shaped domains. All aspects of this anisotropic domain-wall evolution could be reproduced by a simulation based on a modified Ginzburg-Landau-type soft-spin model.

PACS numbers: 75.60.Ch

The magnetization reversal process in thin films occurs either by nucleation of reversed domains or by the displacement of magnetic domain walls [1]. In the latter case, inhomogeneities in the film act as pinning sites for the domain walls and, consequently, have a strong influence on the magnetic domain shape and the dynamics of the magnetization reversal. These inhomogeneities are formed by crystallographic defects or deviations of the film morphology from an ideal atomically flat surface. In general, the extent to which the films' microstructure, as opposed to their intrinsic properties, is affecting the domain structure is difficult to quantify. This is due to the strong interrelationship of these effects. In previous investigations of magnetization processes these influences were modeled by introducing a distribution of coercive fields, thus leaving the actual mechanism of the pinning unspecified [2,3]. A more precise picture of the importance of the microstructure can be developed by introducing well-controlled defects which allow the subsequent identification of their effect on the domain structure. As a model system, one might regard an epitaxial thin magnetic film on a substrate with a predefined defect structure, e.g., a regular array of step edges. In order to visualize the domain structure by means of the magneto-optical Kerr effect the use of Co-based ultrathin magnetic films with perpendicular anisotropy and large domain sizes is advantageous [1,3–8]. In the following, we show that by using vicinal MgO(111) substrates for ultrathin Pt/Co(0.3 nm)/Pt heterostructures, characteristic anisotropic domain shapes are obtained which can be explained and modeled as being caused by the regular arrangement of step edges.

The Pt/Co/Pt(111) trilayers were epitaxially grown in a high-vacuum system onto MgO(111) substrates by sequential dc magnetron sputtering from different targets. The trilayers consist of a 4-nm thick Pt buffer followed by the magnetic Co layer and a Pt capping layer with a thickness of typically $t_{\mathrm{Co}} = 0.3$ nm and $t_{\mathrm{Pt}} = 1.8$ nm, respectively. Prior to growth, a high pressure polishing procedure was applied yielding a highly ordered substrate surface and giving rise to long-range ordered film growth with lateral crystalline coherence lengths above 450 nm [9,10]. The rms roughness of the individual layers as determined by x-ray reflectivity measurements are $\sigma_{\mathrm{Pt}} = 0.05$ nm and $\sigma_{\mathrm{Co}} = 0.2$ nm, respectively. In order to obtain a well-defined tilt of the substrate surface with respect to the MgO{111} planes, a precise tolerance of the substrate holder during the polishing procedure was introduced. The miscut values which can thereby be achieved vary between 0.5° and 1.5°. As a further consequence of the substrate treatment, the surface shows a pyramidal shape with three facets of equal tilt with respect to the (111) plane. These facets are oriented parallel to the $\langle 11\bar{2}\rangle$ directions of the MgO (see Fig. 1).

The magnetization reversal of the samples was analyzed using an optical polarization microscope in the polar configuration. In Fig. 1 the dark regions represent the reversed magnetic domains generated in a field of −750 Oe which was applied for 1 s. The domains reveal an anisotropic shape whose actual form depends on the miscut facet the domains are nucleating on. In contrast, for trilayers grown on MgO(111) with negligible miscut the domains reveal a circular (isotropic) shape, in accordance with previous results for Co-Pt alloy films [6,8]. The origin of the systematic anisotropic domain shape is given by the microstructure of the vicinal substrate surface. The time

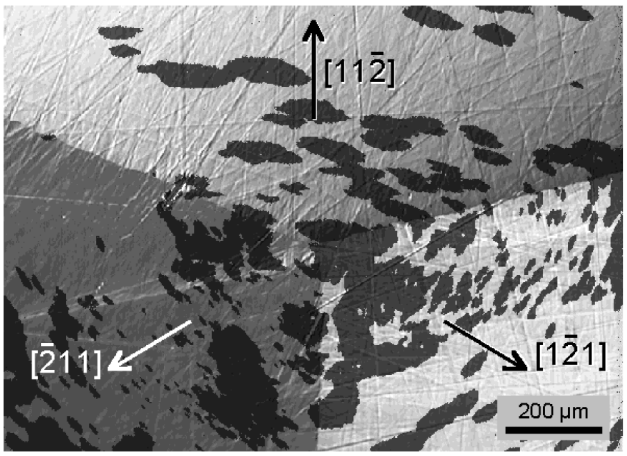

FIG. 1. Superposed optical image of the film surface structure (phase contrast mode) and the magnetic domain pattern (polarization mode) taken during a magnetization reversal process. The scratches at the surface are due to MgO crystallites being abraded from the facet edges during the substrate polishing process.

 0031-9007/00/84(6)/1312(4)$15.00

evolution of the magnetization reversal in any single facet, as shown in Fig. 2, further elucidates this mechanism. Starting from the nucleation sites, which appear to be hard nucleation centers, the domains expand only along the $[\bar{2}11]$ and the $[1\bar{2}1]$ directions, giving rise to a typical triangular domain shape throughout the whole facet.

In the following, we wish to develop a microscopic description that contains the salient features of the influence of the microstructure on the magnetic domain-wall movement. A surface miscut induces the formation of terraces separated by step edges. The density of step edges is determined by the magnitude of the miscut. The step height can be monoatomic or, in the case of step bunching, can comprise several unit cells of the substrate. The presence of terraces results in a surface potential which affects the diffusion of atoms deposited on the surface. The Ehrlich-Schwoebel barrier [11] leads to an increased reflection of the diffusing atoms on downward step edges resulting in a net flux towards the upward step edges. Thus, for coverages in the submonolayer regime and sufficient mobility, this potential gives rise to the accumulation of adatoms in the vicinity of the step edges and a depletion towards the middle of the terraces. In the present case, a magnetic Co monolayer is deposited onto a single-crystalline Pt buffer whose surface ideally is a replica of the substrate's surface microstructure. Following the arguments given above, the concentration of Co atoms is significantly enhanced at the step-edge positions (as schematically shown in the inset of Fig. 3). This modulation of the Co-layer thickness results in a decrease of the effective anisotropy constant K_{eff} of the magnetic film in the vicinity of the steps. Since the spins at the center of a Bloch-like domain wall are aligned parallel to the film plane, the system's energy is minimized if the walls are located at the step edges. Consequently, the thickness gradient of the Co layer results in an energy gradient for the domain-wall position across the terraces. This explains qualitatively the observed anisotropic movement of the domains walls antiparallel to the miscut direction. In excellent agreement with the observations made for Co growth on Pt(111) [12], we observe anisotropic domain-wall movement only for Co coverages below three monolayers up to which thickness Co grows layer by layer. For Co thicknesses larger than three monolayers, strain relaxation causes three-dimensional growth, and circular magnetic domain shapes are observed.

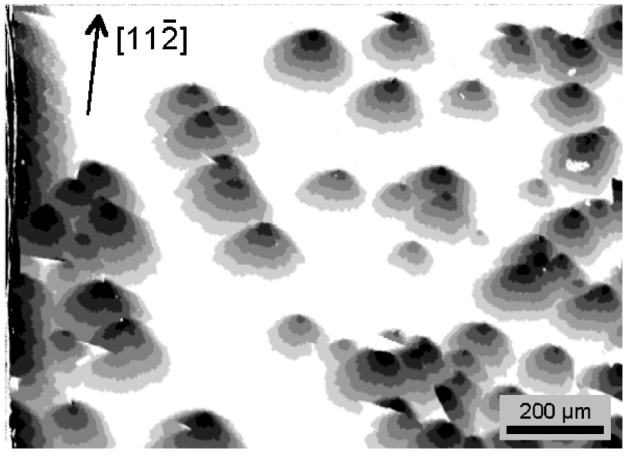

FIG. 2. Kerr image on one miscut facet of the magnetization reversal in a field of -750 Oe. Five images are superposed which were subsequently recorded every 0.25 s. They show the time evolution of the reversed magnetic domains.

For a more quantitative explanation of the anisotropic domain shape, further arguments are needed which will be given by a numerical treatment. This numerical simulation is based on a model which describes the perpendicular spins of the ferromagnet by a mesoscopic nonconserved order parameter $\phi(\vec{r}, t)$. The Ginzburg-Landau Hamiltonian of this Ising-like system reads as [13]

$$\mathcal{H} = \int d^3r \Big(-\frac{a}{2}\,\phi(\vec{r},t)^2 + \frac{b}{4}\,\phi(\vec{r},t)^4 + \frac{J'}{2}[\nabla\phi(\vec{r},t)]^2 - [H + B(\vec{r}) + G(\vec{r})]\phi(\vec{r},t)\Big). \quad (1)$$

Here, the order parameter interacts with an external homogeneous magnetic field H and a static random field $B(\vec{r})$ representing the system's disorder. $J' > 0$ denotes the

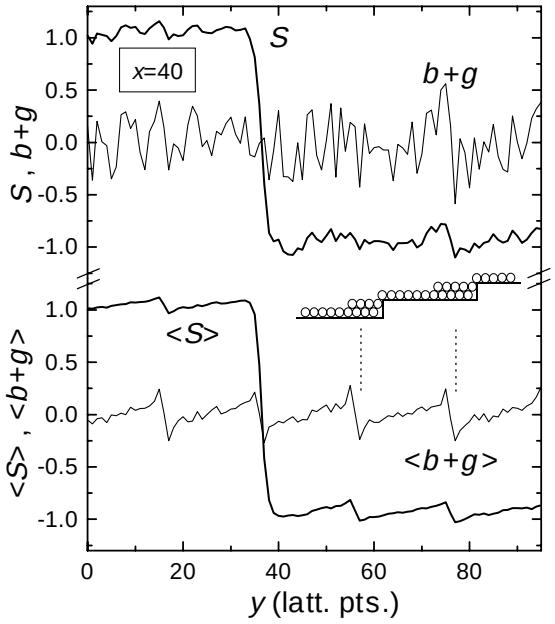

FIG. 3. Numerical simulation (80×150 points) of a magnetic domain wall in the pinned state. The upper graph shows the magnetic system for an arbitrary fixed position x along the step edges. The lower curves show the spins and the pinning fields averaged over all x values. In the inset the relationship between the thickness gradient of the magnetic layer and the resulting pinning field g is shown schematically.

coupling constant between the spins. Supplementing former isotropic treatments [14], we introduce an additional static field $G(\vec{r})$ which reflects the effect of the step edges on the magnetic system. The evolution of the order parameter is assumed to follow a Langevin dynamics at zero temperature:

$$\gamma \frac{\partial \phi(\vec{r},t)}{\partial t} = -\frac{\partial \mathcal{H}}{\partial \phi(\vec{r},t)}, \tag{2}$$

with the system's relaxation time proportional to γ. An application of this model is also possible at finite temperatures, since the arguments given above do not depend on the influence of thermal energies on the domain shape.

For the numerical simulations the continuous fields are rescaled appropriately and discretized to a lattice $\{\vec{l}\}$ which, for simplicity, we choose to be square with a lattice constant c [14,15]. In our case, the discrete version of the Hamiltonian takes the form

$$\mathcal{H} = \sum_{\vec{l}} \frac{u_0}{4}(S_{\vec{l}}^4 - 2S_{\vec{l}}^2) - J\sum_{\vec{l},\vec{l}'}(S_{\vec{l}}S_{\vec{l}'} - z\delta_{\vec{l},\vec{l}'}S_{\vec{l}}^2) - \sum_{\vec{l}}[H + B_{\vec{l}} + G_{\vec{l}}]S_{\vec{l}}, \tag{3}$$

where $\vec{l}'$ are next neighbors to $\vec{l}$, and z is the number of next neighbors. The order parameter ϕ is rescaled ($u_0 = a = b$, $J = J'/c^2$) and is now given by the "soft Ising spins" $S_{\vec{l}}$. Integration of the accordingly modified relaxation Eq. (2) yields a set of difference equations for every spin,

$$S_{\vec{l}}(\tau + \Delta\tau) = S_{\vec{l}}(\tau) + \Delta\tau\Big[-u[S_{\vec{l}}^2(\tau) - 1]S_{\vec{l}}(\tau) + \sum_{\vec{l}'} S_{\vec{l}'}(\tau) - zS_{\vec{l}}(\tau) + h + b_{\vec{l}} + g_{\vec{l}}\Big], \tag{4}$$

with the rescaled parameters $\tau = Jt/\gamma$, $u = u_0/J$, $h = H/J$, $b_{\vec{l}} = B_{\vec{l}}/J$, and $g_{\vec{l}} = G_{\vec{l}}/J$. The quenched noise of the system is assumed to have a cutoff white distribution; i.e., the rescaled random fields $\{b_{\vec{l}}\}$ take on values in an interval $[-p, p]$ with equal probability. In total, three parameters enter in the simulation for the isotropic case (without step edges): the "coupling" u, the external field h, and the maximum value of the pinning p.

In the anisotropic case, this has to be augmented by an appropriately chosen form of the fields $\{g_{\vec{l}}\}$. Following the explanation for the anisotropic domain-wall propagation given above, the functional form of the step-edge induced pinning field g is modeled for the nth step line by the real part of a Lorentz-like function,

$$g_n(y) = -d\frac{2\Gamma(y - y_n)}{(y - y_n)^2 + \Gamma^2}, \tag{5}$$

where $y_n - w/2 < y \le y_n + w/2$. Here, y_n is the y coordinate of the nth step and w is the vertical distance between the steps. The minimum of the Lorentz curve corresponds to the accumulation of Co atoms in the vicinity of a step edge which affects the magnetic domain walls as a pinning potential. The height of the pinning potential is determined by d and its width is given by Γ. In analogy to the maximum value p of the random pinning field, d enters as a further simulation parameter. It determines the magnitude of the pinning field in the vicinity of the step edges.

In the following numerical simulations we show that the introduction of the pinning field g leads to an effective anisotropic pinning behavior of the system even for small values of d. The choice of the rescaled isotropic parameters ($h = 0.1$, $u = 0.9$, and $p = 0.4$) is based on the optimization for the isotropic problem. These isotropic simulations yield domain-wall morphologies which exhibit scaling properties identical to those experimentally observed for circular domain patterns. The result of these investigations will be published elsewhere. The maximum value of the pinning field g is chosen to be slightly smaller than the maximum random field ($d = 0.25$).

Figure 3 shows the result of a two-dimensional (80×150 lattice sites) simulation in which the step edges are arranged in rows along the x direction with a vertical distance of $w = 20$ lattice points. The simulation shows the magnetic system in the pinned state; i.e., the domain wall does not change its position, even for long iteration times. In the upper graph the spin function S and the sum of the pinning fields $b + g$ are drawn as a function of y for an arbitrarily chosen fixed x position along the step edges. The jaggedness of the random field b conceals the field g so that the pinning fields do not show a significant periodicity. The reason why the system remains in the pinned state only becomes apparent if S and $b + g$ are averaged over all x (lower graph in Fig. 3). In this case the periodic structure of g becomes visible and the domain walls

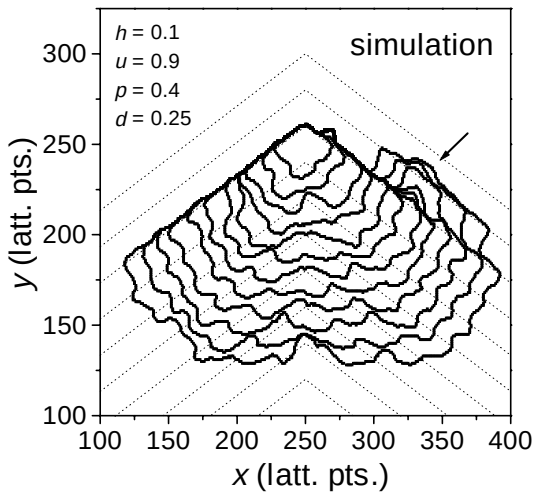

FIG. 4. Simulation of the domain-wall propagation. The dotted lines indicate the centers of the additional pinning field g which represents the influence of the step edges on the magnetic system.

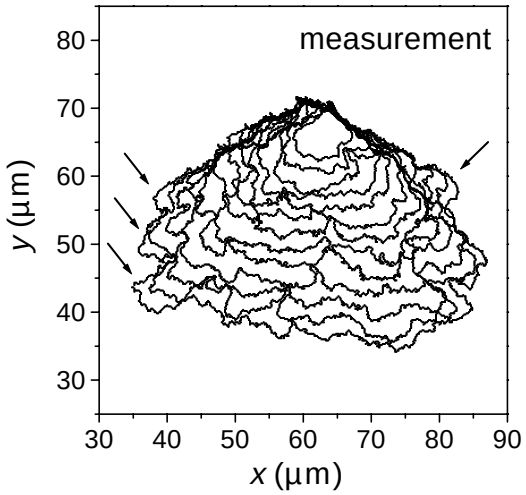

FIG. 5. Digitized images during a magnetization reversal in a field of −660 Oe. The domain-wall positions were recorded every 0.5 s.

are located at the minima of the pinning potentials. Apparently, due to their elastic properties the magnetic domain walls are trapped by elongated structures even if the pinning forces are weaker than the random pinning fields arising from disorder. This elastic property of the domain walls is a direct consequence of the spin-spin interaction. The assumption of a rowlike distribution of the step edges alone cannot explain the anisotropic shape of the domains. In order to reproduce the observed domain shapes in the simulation, the actual planar arrangement of the step edges on MgO has to be implemented in Eq. (5). It is well known that the annealed surface of MgO(111) splits up into {100} facets [16,17]. Therefore, a vicinal (111) surface will form step edges parallel to ⟨100⟩. The projections of these ⟨100⟩ directions onto the substrate surface are parallel to $\langle\bar{2}11\rangle$. This faceting of diagonal step edges is in analogy to the formation of macroscopic miscut facets shown in Fig. 1. Consequently, the faceting of the step edges is modeled for the simulation by a fishbonelike arrangement of step lines forming an angle of 120° (dotted lines in Fig. 4). The coordinates of the nth step edge is then determined by $y_n(x) = y^0 - nw - |x - x^0| \tan 30°$.

Figure 4 shows the result of a simulation on a 500 × 500 lattice with this type of step-edge arrangement. The simulation shows all relevant features of the experimentally observed domain patterns (Fig. 5): The domain walls have two preferential directions for propagation, giving rise to the characteristic triangular domain shape. This is caused by the diagonal "channels" between the step lines in which the domain wall can move easily. The edge of the topmost channel works as a guiding line for the domain-wall movement. At some position (marked with an arrow in Fig. 4) the domain wall overcomes this line and enters the adjacent channel. These "protuberances" are also seen in the measurements (marked positions in Fig. 5).

In conclusion, we showed that the magnetic domain-wall motion in ultrathin films with perpendicular anisotropy is very sensitive to elongated pinning structures such as substrate induced step edges. The observed anisotropic wall propagation is due to a thickness gradient of the magnetic layer in the vicinity of the step edges. The characteristic triangular domain shapes directly emerge from the actual planar arrangement of the steps. The domain-wall evolution can be simulated successfully using a Ginzburg-Landau-like "soft spin model" augmented by an additional pinning term which describes the effective pinning force due to a thickness gradient of the magnetic layer.

The authors wish to thank H. J. Elmers for fruitful discussions.

[1] J. Pommier, P. Meyer, G. Pénissard, J. Ferré, P. Bruno, and D. Renard, Phys. Rev. Lett. **65**, 2054 (1990).
[2] P. Bruno, G. Bayreuther, P. Beauvillain, C. Chappert, G. Lugert, D. Renard, J. P. Renard, and J. Seiden, J. Appl. Phys. **68**, 5759 (1990).
[3] J. Ferré, V. Grolier, P. Meyer, S. Lemerle, A. Maziewski, E. Stefanowicz, S. V. Tarasenko, V. V. Tarasenko, M. Kisielewski, and D. Renard, Phys. Rev. B **55**, 15 092 (1997).
[4] V. Grolier, J. Ferré, M. Galtier, and M. Mulloy, J. Appl. Phys. **76**, 6983 (1994).
[5] J. Ferré, J. P. Jamet, J. Pommier, P. Beauvillain, C. Chappert, R. Mégy, and P. Veillet, J. Magn. Magn. Mater. **174**, 77 (1997).
[6] U. Nowak, J. Heimel, T. Kleinefeld, and D. Weller, Phys. Rev. B **56**, 8143 (1997).
[7] S. Lemerle, J. Ferré, C. Chappert, V. Mathet, T. Giamarchi, and P. Le Doussal, Phys. Rev. Lett. **80**, 849 (1998).
[8] M. Jost, J. Heimel, and T. Kleinefeld, Phys. Rev. B **57**, 5316 (1998).
[9] P. Haibach, J. Köble, M. Huth, and H. Adrian, Thin Solid Films **336**, 168 (1999).
[10] P. Haibach, J. Köble, M. Huth, and H. Adrian, J. Magn. Magn. Mater. **198–199**, 752 (1999).
[11] G. Ehrlich and F. G. Hudda, J. Chem. Phys. **44**, 1039 (1966); R. L. Schwoebel, J. Appl. Phys. **40**, 614 (1969).
[12] P. Grütter and U. T. Dürig, Phys. Rev. B **49**, 2021 (1994).
[13] P. C. Hohenberg and B. I. Halperin, Rev. Mod. Phys. **49**, 435 (1977).
[14] M. Jost and K. D. Usadel, Phys. Rev. B **54**, 9314 (1996).
[15] K. D. Usadel and M. Jost, J. Phys. A **26**, 1783 (1993).
[16] V. E. Henrich, Surf. Sci. **57**, 385 (1976).
[17] R. Plass, J. Feller, and M. Gajdardziska-Josifovska, Surf. Sci. **414**, 26 (1998).